Joining and Brazing

A STUDY OF MICROSEGREGATION EFFECTS IN TIG AND LASER BEAM WELDS OF AN Al-Cu-Mg ALLOY

Andrew F. NORMAN and Philip B. PRANGNELL

Manchester Materials Science Centre, University of Manchester / UMIST
Grosvenor Street, Manchester, M1 7HS, U.K.

ABSTRACT The techniques of TIG and laser beam welding were used to produce autogenous welds for an Al-Cu-Mg alloy. Composition profiles were measured across the dendrite side arms which followed a Scheil type segregation behaviour, in which there is negligible back diffusion in the solid. The core concentrations of the dendrite side arms were more than twice that predicted by the equilibrium phase diagram and, for the TIG welds, were found to increase with welding speed. In contrast, core concentrations for the laser welds appeared to be independent of the welding speed. The increase in core composition in the side arms was related to the formation of significant undercoolings ahead of the primary dendrite tip, which enriched the liquid surrounding the dendrite side arms.

Keywords: *TIG, Laser Beam Welding, Microsegregation, TEM, Al-Cu-Mg Alloys.*

1. INTRODUCTION

In welding processes such as TIG and laser beam, a good understanding of how the weld microstructure and adjacent heat affected zones (HAZs) form is required if the optimum performance of the alloy is to be achieved [1-3]. This is particularly important for the welding of age hardenable aluminium alloys, such as AA2000 and AA7000 series, as the severe thermal cycles that occur in welding can induce a variety of complex metallurgical reactions in the parent metal [4,5].

Whilst the development of grain structures in Al alloy TIG welds is relatively well understood [2,6], little research has been published on the grain structures formed in Al alloy laser welds. Furthermore there has only been a limited number of studies concerning the microsegregation behaviour within grains of Al alloy welds in general. An understanding of the redistribution of solute during the solidification of the weld metal is particularly important in heat treatable alloys, such as AA2024, as the weld metal strength will depend on the solute supersaturation, which determines the subsequent ageing response and yield strength. It is equally important to be able to predict the macroscopic grain structure, dendrite arm spacing within the grains, and the volume fraction of eutectic formed, which will dominate the toughness and ductility. A number of workers have established that a relatively simple approach, based on estimating the cooling rate, can be used to reliably predict the dendrite arm spacings in simple model aluminium alloys [7], but it is only recently that this has been attempted with more complex alloys of near commercial composition [2]. Furthermore, there is only limited experimental data available in the literature comparing measurements of solute profiles across dendrites in welds, to models of solute redistribution [1,8]. Conflicting results exist between measured solute profiles with some workers reporting a Scheil behaviour [9], where there is effectively no diffusion in the solid phase, and other profiles based on the model of Brody and Flemings [10], where there is limited back diffusion in the solid.

In this paper a series of autogenous welds were produced using both TIG and laser beam welding of the commercial aluminium alloy AA2024. This allowed a wide range of welding speeds and power inputs to be considered. The welds were characterised using optical metallography to reveal the different macroscopic grain structures, produced with the different welding conditions. Transmission Electron Microscopy (TEM) was used to measure the effect of each welding process

on the segregation behaviour of the major alloying element in AA2024 and the results are compared to existing models for the prediction of microsegregation behaviour in welds.

2. EXPERIMENTAL

The commercial aluminium alloy AA2024 (Al - 4.4 wt.% Cu - 1.5 wt.% Mg - 0.8 wt.% Mn + Fe and Si impurities) was TIG and laser beam welded using the conditions given in Table 1. The sheet thickness was 1.6 mm and a simple butt geometry was used for each experiment. For the TIG welds, the speeds considered were in the range 0.7 to 2.5 cm s^{-1}, and as the welding speed was increased, the welding current was also increased to just maintain full penetration. For the laser welding, a YAG laser was used to produce welds in the range 3.3 to 10 cm s^{-1} requiring a laser power of between 2 and 4 kW to achieve full penetration. After welding, each sample was sectioned, mounted and examined using conventional optical metallography. Samples for TEM examination were prepared from the welds by punching 3 mm discs from different positions in the weld sample. The discs were ground to a thickness of ~ 100 μm and jet-polished using a solution of 30 vol.% Nitric Acid in Methanol at –30°C and 12 V. The foils were examined in a Philips CM200 analytical TEM operated at 200 kV. Quantitative EDX analysis was used to measure the solute profiles in several dendrite side arms for each welding speed.

Table 1: Welding conditions and calculated values of power input and thermal gradient (G_L).

Welding Speed (cm s^{-1})	Current (TIG) (A)	Power (W)	G_L (K cm^{-1})	G_L/R	$G_L.R$ (K s^{-1})
0.7	100	630[a]	7.42[b]	10.0	519
1.3	130	819[a]	8.15[b]	6.0	1059
1.9	160	1008[a]	7.87[b]	4.1	1495
2.5	190	1197[a]	7.34[b]	2.9	1835
3.3	-	2000	25.1[c]	7.6	8283
6.6	-	3000	36.0[c]	5.45	23760
10.0	-	4000	41.0[c]	4.1	41000

[a]calculated from $Q = \eta IV$ where Q is the total heat input, V is the welding voltage, and η is taken to be 0.70 [11], [b]estimated from the Rosenthal thin plate solution [2], [c]calculated using the thermal model in Ref. [3].

3. RESULTS AND DISCUSSION

3.1 Microstructural Observations

In an earlier paper [2], we reported observations on the macroscopic grain structures that occur in the fusion zone of autogenous AA2024 TIG welds. At low welding speeds and power inputs, the fusion zone consisted of columnar-dendritic grains, which grew along the centre of the weld in the direction of the heat source, whereas at high welding speeds and power inputs, the central region of the fusion zone was replaced with an equiaxed-dendritic structure with an average grain size of ~ 250 μm (Fig. 1a). For the laser welds, equiaxed-dendritic grain structures were observed along the weld centreline which prevailed throughout the length of the welds for the complete range of welding conditions examined (Fig. 1b). In the laser welds, the average grain size along the weld centreline was ~ 100 μm.

The transition from columnar to equiaxed grains in TIG welding has been observed by a number of researchers [2,4,6]. The formation of an equiaxed region in the centre of the weld can be expected, providing the combination of correct thermal conditions for the nucleation and growth of new grains (an undercooled region ahead of the solid/liquid interface), and the presence of stable

nuclei in the liquid. The stable nuclei are thought arise from a combination of dendrite or grain fragments which survive in the undercooled region of the melt pool, and TiB_2 particles which are present in the original base alloy to control the grain structure during casting [2]. As the welding speed is increased, significant undercoolings can develop in the liquid ahead of the growing columnar front. This allows the nuclei present in the weld pool to grow into new grains and block the advancing columnar front [12]. The values of thermal gradient (G_L) and growth rate (R) have been calculated for both the TIG and laser beam welded samples, at the trailing edge of the weld pool along the weld centreline (Table 1). For this position in the weld pool, the values of G_L and R are quite different for the two processing techniques. However, at high welding speeds the ratio of G_L/R for the two techniques are in a similar range, suggesting that the formation of equiaxed grains should be favoured in both welding processes, as can be seen in Figure 1.

Although the calculated G_L/R ratios are very similar for the two welding processes considered in this work, this will not be the case for the product of the components, namely the cooling rate ($\varepsilon = G_L.R$). For TIG welds, dendrite arm spacings between 3 and 6 μm were measured for the range of welding speeds, along the weld centreline. In contrast to this, the dendrite spacings measured in the laser welds are much finer, varying from 2.4 μm for the slowest welding speed (3.3 cm s^{-1}) to 1.6 μm for the highest speed (10.0 cm s^{-1}). The dendrite secondary arm spacing can be estimated using the simple expression, $\lambda_2 = a(G_L R)^{-n}$, where a and n are constants whose values depends on the alloy system. The values of a = 50 and $n = -1/3$ have been used to successfully predict the secondary arm spacing in binary Al-Cu alloys, for cooling rates in a similar range to those considered in this work (i.e., 1 to 10^5 K s^{-1} [7]). Using these values, the calculated secondary arm spacings are plotted in Fig. 1c together with the measured spacings, taken from the weld centreline. Fig. 1c shows that as the welding speed is increased, both the measured and calculated secondary arm spacings decrease, and that there is good agreement between the measured and calculated values over the complete range of processing techniques.

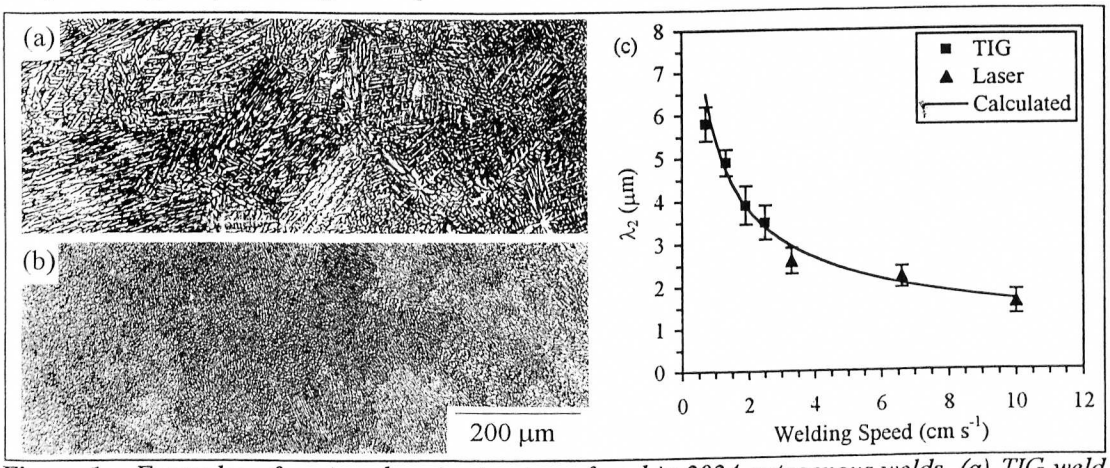

Figure 1: Examples of equiaxed grain structures found in 2024 autogenous welds. (a) TIG weld, speed = 2.5 cm s^{-1}, and (b) Laser weld, speed = 10.0 cm s^{-1}. (c) plot of dendrite secondary arm spacing vs. welding speed.

3.2 Microsegregation Behaviour

TEM was used to study the segregation behaviour of the major alloying element in 2024, namely Cu, for the different welding techniques (although Mg is also a major alloying element in 2024, it could not be reliably analysed due to the overlap with the Al K_α peak). Solute profiles were produced across many individual dendrite side arms for both TIG and laser welded samples. Details of the analysis procedure are given in [2]. Fig. 2a shows that the lowest Cu concentration always occurs in the centre of the dendrite arm (TIG and laser beam) and that the Cu concentration

increases towards the interdendritic boundary. These results demonstrate that the segregation behaviour is more similar to the scenario envisaged by Scheil [9], where there is negligible back diffusion in the solid, rather than that expected by the Brody and Fleming model [10]. The initial transient in solute content predicted by Brody and Flemings was not observed.

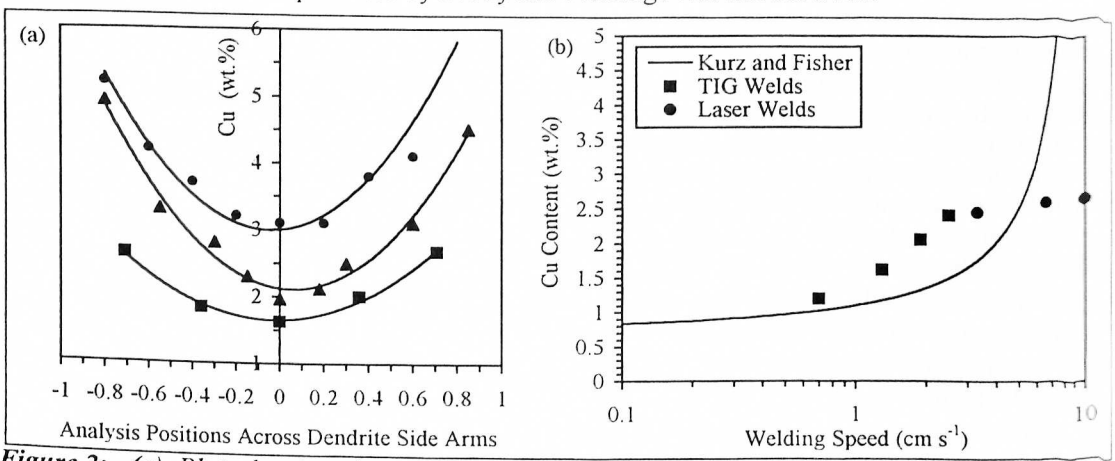

Figure 2: *(a) Plot showing the variation in Cu concentration across dendrite side arms for different welding processes (■ - 0.7 cm s^{-1} (TIG), ▲ - 1.3 cm s^{-1} (TIG), ● - 6.6 cm s^{-1} (Laser)) . (b) plot of minimum Cu concentration vs. welding speed.*

The Scheil equation for solute partitioning (which best represents the trends shown in our data) is given by; $C_S = C_0k(1-f_S)^{k-1}$, where C_S is the solid composition, C_0 is the initial alloy composition, f_S is the fraction of solid and k is the partition coefficient. The Scheil equation is based on the assumptions that there is complete mixing in the liquid state (uniform liquid composition), local equilibrium prevails at the solid/liquid interface, and that there is negligible solid-state diffusion. Whether or not there is a significant contribution of solid state diffusion to the solute redistribution process can be estimated from the dimensionless parameter [10]; $\alpha = (D_S t_f)/\lambda_2^2$, where D_S is the solid diffusivity of the solute and t_f is the local time of freezing. For the welds produced in this work, the values of t_f are in the range 0.01 to 0.2 secs. which produces an α parameter in the range 2.4×10^{-3} to 1×10^{-4}. As it can be shown that solid state diffusion during freezing only begins to become an important factor in the solute redistribution process for values of $\alpha > 0.1$ [10], the composition profiles measured in this work should fall close to the prediction of the Scheil equation.

The effect of welding speed on the core composition of the dendrite side arm was investigated in more detail by analysing the centre of several side arms for each welding speed (TIG and laser beam). As there are significant problems associated with the random sectioning of dendrite side arms during the preparation of TEM thin foils, the minimum observed concentration is plotted in Fig. 2b for the two welding techniques. The data in Fig. 2b shows that, for the TIG samples, the dendrite core composition increases as the welding speed is increased. This is not the case for the laser welds where the measured core concentrations show almost no variation with welding speed. The reasons for this behaviour are explained in more detail below.

According to the Scheil equation, the starting solid composition (C_S) is given by the product of C_0 and k, i.e. for an alloy composition of 4.46 wt.% Cu, a core composition of 0.76 wt.% Cu should be produced, which is much less that that observed experimentally in Fig. 2b. Furthermore, the Scheil equation suggests that the starting composition should be independent of the welding speed which is clearly not the case. Similar experimental observations have been made by Brookes and Baskes [8] who studied GTA binary Al-Cu welds containing between 1 and 2 wt.% Cu (much lower than the compositions studied here). They also observed core concentrations between $2C_0k$ and

$3C_0k$, at similar speeds, which is in good agreement with the core concentrations measured in this work.

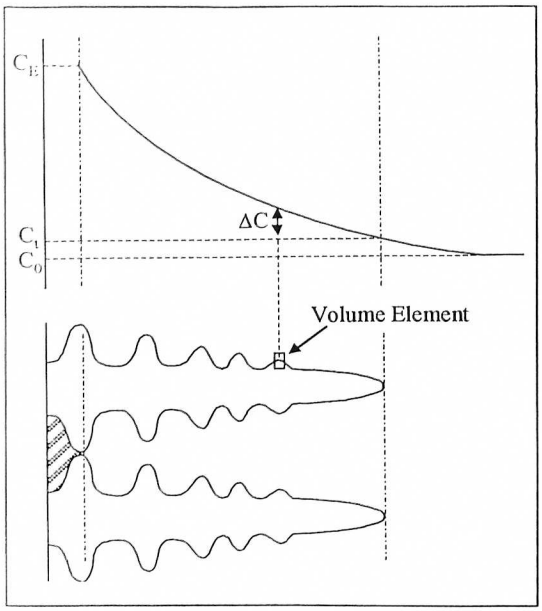

Figure 3: Schematic diagram illustrating a possible solute profile for the growth of dendrites.

A possible solute profile for the growth of dendrites is shown schematically in Fig. 3. In this figure, the composition in the bulk of the liquid is given by C_0. It is possible that for the range of welding speeds considered in this work, significant undercoolings can be achieved at the primary dendrite tip which will enrich the liquid ahead of the tip (i.e., produce the composition of C_t in Fig. 3). Microstructural observations have shown that a significant volume fraction of eutectic phases are formed in the mushy zone at the end of solidification, i.e. at the root of the dendrites in the interdendritic regions. This suggests that in the interdendritic regions, the solute profile will change as it moves through the mushy zone, from C_t to C_E, the eutectic composition - as shown in Fig. 3. Therefore in the regions where the secondary arms form, the local liquid composition is enriched with solute to a level somewhere between C_t and C_E, i.e. the core concentration of the dendrite side arm will be given by $k(C_t + \Delta C)$, where ΔC depends on the relative distance back from the tip where the secondary arms form (of the order of 2 to 3 secondary arm spacings [10]).

In recent years, models have been developed which allow the tip undercooling to be estimated for different growth conditions. For example, Burden and Hunt [13], derived an expression for tip undercooling as a function of the growth velocity, thermal gradient and tip radius. To obtain a unique solution, Burden and Hunt used the criteria that the dendrite always grows at the minimum undercooling. More recently, Kurz and Fisher [14] have pointed out that the minimum undercooling criteria underestimates the change in tip temperature, and have instead, used the criteria that the tip radius is equal to the wavelength of instability of the interface. In both approaches, the tip temperature is dominated by the growth velocity, rather than the thermal gradient, when the growth velocities are high ($> 10^{-3}$ cm s^{-1}). Both approaches show that the tip undercooling starts to rapidly increase at velocities of $\sim$ 1 cm s^{-1} although the Kurz and Fisher model predicts that this will occur at a greater rate. This variation in tip undercooling has been translated to a core composition for the growth of primary dendrites in a binary Al - 4.46 wt.% Cu alloy, and the data is shown in Fig. 2b together with the measured values for the secondary arms.

By assuming that the primary tip velocity is the same as the welding speed, the model of Kurz and Fisher demonstrates that as the welding speed is increased, so the primary tip concentration also increases, i.e. in agreement with the trends of this work. However the measured and predicted values deviate significantly at high welding speeds, particularly for the laser welds. Clearly, the assumption that the primary tip grows at the same velocity as the welding speed is only realistic when a directional columnar solid/liquid interface is observed, i.e. for axial grain structures. For equiaxed growth (observed in all laser weld samples), it is likely that the tip velocity will not equal the welding speed, but in fact be at a somewhat lower value. Therefore it is possible that for the laser welding samples, where severe turbulence is experienced in the weld pool, the growth velocity of the equiaxed grains is largely independent of the welding speed, and gives rise to the plateau seen in Fig. 2b.

In the above analysis, an argument not considered is that the increase in core composition of the secondary arms is attributed to the undercoolings developed at the secondary arm tip. The tip velocity for a growing secondary arm can be crudely estimated by dividing the arm spacing by the local freezing time. For the welds examined in this work, this translates to a growth rate of ~ 10^{-2} cm s^{-1}, which if applied to the primary tip model, gives a negligible undercooling.

4. CONCLUSIONS

1. Composition profiles were measured in the TEM which showed that the microsegregation of Cu in TIG and laser welds followed the behaviour envisaged by Scheil, with negligible back diffusion occurring in the solid.
2. For TIG welding, the core concentration of the dendrite side arms increased with welding speed and were more than twice that predicted by the equilibrium phase diagram. However, this was not the case for the laser welds where a plateau of Cu concentration was observed.
3. The increase in core composition in the side arms was related to the formation of significant undercoolings ahead of the primary dendrite tip, which enriched the liquid surrounding the dendrite side arms.
4. For the highest welding speeds, equiaxed grain structures were observed, which limited the growth velocity of the primary dendrite tip.

5. ACKNOWLEDGEMENTS

This work was supported by the EPSRC under the IMI Programme, Grant: GR/K66901, and is released with the kind permission of the following partners: British Aerospace, Short Brothers, DERA, Rolls Royce, British Aluminium, TWI, University of Liverpool, Cranfield University, and the University of Essex.

6. REFERENCES

[1] S.A. David and J.M. Vitek: Internat. Mater. Rev., 34 (1989), 213.
[2] A.F. Norman, V. Drazhner and P.B. Prangnell: submitted to Mater. Sci. Eng. A.
[3] A.F. Norman, R. Ducharme, A. Mackwood, P. Kapadia and P.B. Prangnell: Science and Technology of Welding and Joining, in press.
[4] S. Kou: Welding Research Council Bulletin, 320 (1986), 1.
[5] A.F. Norman, V. Drazhner, N. Woodward and P.B. Prangnell: Proc. 7th Int. Conf. On Joints in Aluminium (INALCO '98), TWI, Cambridge, 1998, to be published.
[6] T. Gahana, B.P. Pearce and H.W. Kerr: Met. Trans. A, 11 (1980), 1351.
[7] H. Jones: Monograph No.8, Institute of Metallurgists (1982).
[8] J.A. Brookes and M.J. Baskes: Advances in Welding Science and Technology, (edited by S.A. David), Metals park, OH, ASM International, p. 93 (1987).
[9] E. Scheil: Z. Metallkd., 34 (1942), 70.
[10] H.D. Brody and M.C. Flemings: Trans. AIME, 236 (1966), 615.
[11] Ø. Grong: Metallurgical Modelling of Welding, (edited by H.K.D.H. Bhadeshia), Institute of Materials (1994).
[12] J.D. Hunt: Mater. Sci. Eng., 65 (1984), 75.
[13] M.H. Burden and J.D. Hunt: J. of Crystal Growth, 22 (1974) 109.
[14] W. Kurz and D.J. Fisher: Acta Metall., 29 (1981), 11.